Modulated structures in the Ising model with competing interactions on the Cayley tree

J. G. Moreira
Departamento de Física, Universidade Federal de Minas Gerais, Caixa Postal 702, 30161, Belo Horizonte, Minas Gerais, Brazil

S. R. Salinas
Instituto de Física, Universidade de São Paulo, Caixa Postal 20516, 01498, São Paulo, São Paulo, Brazil
(Received 4 May 1992)

We introduce two analogs of the axial next-nearest-neighbor Ising (ANNNI) model on a Cayley tree. Besides the competing interactions along the branches of the tree, we include a set of pair interactions on the same generation to mimic the ferromagnetic layers of the ANNNI model. In the infinite-coordination limit, the statistical problem is formulated as a discrete, nonlinear, two-dimensional map. The phase diagrams display a Lifshitz multicritical point and many sequences of modulated structures characterized by a principal wave number. At low temperatures, we perform numerical calculations to show the existence of complete devil's staircases. At higher temperatures, the incommensurate structures occupy finite portions of the phase diagrams. We discuss the existence of pinned incommensurate phases. Also, we calculate the Lyapunov exponents of the map to show the presence of chaotic structures, associated with a strange attractor. The main modulated phase of the long-range model under consideration displays a transition between characteristic structures at low and high temperatures.

I. INTRODUCTION

The axial next-nearest-neighbor Ising (ANNNI) model is an Ising spin system on a cubic lattice, with ferromagnetic ($J_0>0$) interactions between nearest neighbors on the x-y planes and competing ferromagnetic ($J_1>0$) and antiferromagnetic ($J_2<0$) interactions between first and second neighbors along the z direction.[1-7] In terms of the temperature T and the parameter $p=-J_2/J_1$, the phase diagram of the ANNNI model displays many complex features, including a variety of modulated structures and some multicritical points, which have attracted the attention of several investigators.[5-7]

Some sophisticated techniques, such as high-temperature[8] and low-temperature[3] series expansions, and Monte Carlo simulations,[1] have essentially confirmed the mean-field picture[2] of the phase diagram of the ANNNI model. The minimization of a layer-by-layer mean-field free energy gives the set of equations[2,9,10]

$$m_j=\tanh[4\beta J_0 m_j+\beta J_1(m_{j-1}+m_{j+1}) +\beta J_2(m_{j-2}+m_{j+2})]\ , \tag{1.1}$$

for $j=1,2,\ldots,N$, where $\beta=(k_BT)^{-1}$, and m_j is the mean-field magnetization per spin on the jth x-y layer of the lattice. At high temperatures a Fourier analysis of this set of equations yields the paramagnetic lines and location of a Lifshitz point.[9] Along the second-order paramagnetic-modulated border, there is a smoothly varying critical wave number (which vanishes at the Lifshitz point). At lower temperatures, however, inside the more interesting region of modulated structures, these equations are no longer amenable to analytical treatments. We then perform a truncation and resort to numerical techniques to find the set of solutions that minimize the free energy.[2,9] It is not difficult to obtain the main commensurate phases (which are characterized by a principal wave number). However, it becomes disappointingly difficult to investigate some details of the phase diagrams, such as the existence of a succession of modulated structures and the dimensionality of the devil's staircases associated with the graphs of the principal wave number as a function of T and p. It should be noted that the fourth-order mean-field difference equations can be written as a four-dimensional area-preserving map.[11] This connection with dynamical systems, however, also leads to a quite difficult numerical problem. The stable orbits of this map are usually unstable solutions of the thermodynamic problem.

Some analogs of the ANNNI model on a Cayley tree, although associated with much simpler mathematical problems, have been shown to display phase diagrams as rich and complex as their counterparts on a Bravais lattice.[12-15] For example, Yokoi, de Oliveira, and Salinas[15] considered the infinite-coordination limit of an Ising model on a Cayley tree with competing ferromagnetic ($J_1>0$) and antiferromagnetic ($J_2<0$) interactions between first and second neighbors, restricted to the radial direction, along the branches of the tree. For a tree of coordination z, in the infinite-coordination limit $z\to\infty$, $J_1\to 0$, $J_2\to 0$, with zJ_1 and z^2J_2 fixed, this basic problem can be formulated in terms of the recursion relations

$$m_j=\tanh\left[\frac{1}{t}m_{j-1}-\frac{p}{t}m_{j-2}\right]\ , \tag{1.2}$$

where $t=(\beta zJ_1)^{-1}$, $p=-(z^2J_2)/(zJ_1)$, and m_j is an effective magnetization per spin associated with the jth generation of the tree. Given the boundary conditions

(which are usually taken as $m_1=m_2=1$), the attractors of the map correspond to solutions on the Bethe lattice, deep inside the Cayley tree. As this two-dimensional map is nonconservative, it becomes relatively easy to perform detailed numerical calculations to study many subtleties of the phase diagram.[15]

In the present paper, we introduce two analogs of the ANNNI model on a Cayley tree. In addition to the competing interactions along the branches of the tree, which are already present in the basic model, we consider a selected number of ferromagnetic ($J_0>0$) interactions between pairs of spins belonging to the same generation and associated with a common ancestor along the tree. With a convenient choice of the interactions, which are meant to mimic the ferromagnetic x-y planes of the ANNNI model on the cubic lattice, the problem can still be formulated as a nonlinear discrete map. In the short-range (SR) model, we choose short-range ferromagnetic interactions along a chain of spins. In the infinite-coordination limit, the map is two dimensional, and the results are not far from the findings for the basic model. The long-range (LR) model includes ferromagnetic interactions of equal strength between all pairs of spins. These models are identical for a tree of coordination $z=3$. As the coordination increases, however, they become quite distinct. In the infinite-coordination limit, the discrete nonlinear map associated with the LR model is still two dimensional, but much harder to analyze.

The layout of this paper is as follows: In Sec. II we define the analogs of the ANNNI model on a Cayley tree of coordination z. The solutions of this general problem are written as a discrete nonlinear map (which becomes two dimensional, and quite simple, in the infinite-coordination limit). Some analytical results for the t-p phase diagrams are obtained in Sec. III. In particular, we obtain expressions for the second-order paramagnetic lines and the location of the Lifshitz multicritical point. In Sec. IV we present some numerical calculations for the two-dimensional map associated with the SR model. We show the existence of complete devil's staircases at low temperatures. At higher temperatures we present numerical evidence to suggest that the incommensurate structures occupy finite portions of the t-p phase diagram. Also, for a certain range of the parameters, we show the existence of chaotic structures associated with a strange attractor of the map. In Sec. V we present some numerical calculations for the LR model. The qualitative results are not far from the SR model in the limit of infinite coordination. A more detailed analysis of the $\frac{1}{6}$ commensurate phase indicates some structural changes with temperature in close connection with recent findings for the ANNNI model. Finally, some conclusions are presented in Sec. VI.

II. FORMULATION OF THE PROBLEM

A Cayley tree is a cycle-free structure as shown in Fig. 1 for coordination $z=4$. The dashed lines indicate the successive generations of this tree. The Ising model on the Cayley tree is given by the Hamiltonian

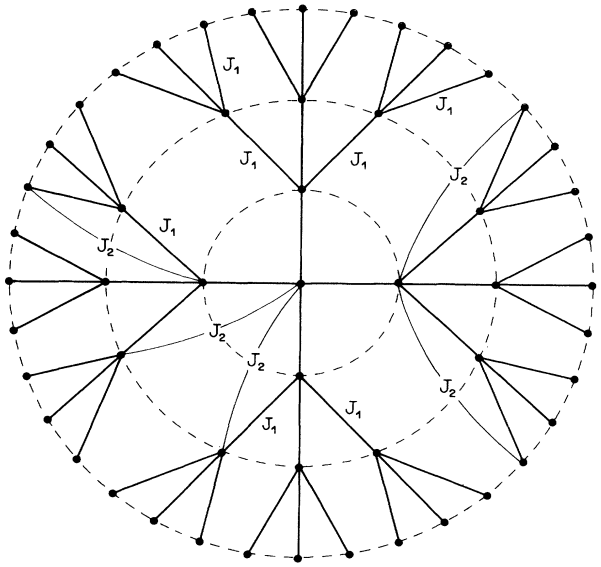

FIG. 1. Three generations of a Cayley tree of coordination $z=4$. The parameters J_1 and J_2 indicate some interactions between first and second neighbors along the branches of the tree.

$$\mathcal{H}=-\sum_{i,j}J_{i,j}S_iS_j-h\sum_i S_i\ , \tag{2.1}$$

where h is an external field, the first sum is over pairs of sites of the tree, and $S_i=\pm1$ for all values of i. In this paper we consider ferromagnetic interactions ($J_1>0$) between first neighbors and antiferromagnetic interactions ($J_2<0$) between second neighbors, along the branches of the tree, in the radial direction (as indicated in Fig. 1). To simulate the in-plane interactions of the ANNNI model, we also consider ferromagnetic couplings ($J_0>0$) between spins belonging to groups of sites of the same generation connected to a common ancestor site of the tree. We study two types of models: (i) the SR model, with nearest-neighbor J_0 ferromagnetic interactions, as illustrated in Fig. 2(a): (ii) the LR model, with long-range J_0 ferromagnetic interactions between spins on all sites belonging to the same generation and connected to a common ancestor, as illustrated in Fig. 2(b).

The partition function of these Ising models is given by

$$Z=\mathrm{Tr}\exp(-\beta\mathcal{H})\ , \tag{2.2}$$

where the trace is a sum over spin configurations. Taking advantage of the structure of the tree, we can perform separate sums over spins belonging to successive generations.[13] Considering Fig. 2, we can write the partial trace

$$f(S_A,S_B)=\sum_{\{S_i\}}\exp\left\{(K_1S_A+K_2S_B+H)\sum_{i=1}^{z}S_i+K_0\sum_{i,j}S_iS_j\right\}\ , \tag{2.3}$$

where $K_0=\beta J_0$, $K_1=\beta J_1$, $K_2=\beta J_2$, and $H=\beta h$. The sum over the sites i,j depends on the particular model (SR or LR) under consideration. This function can also

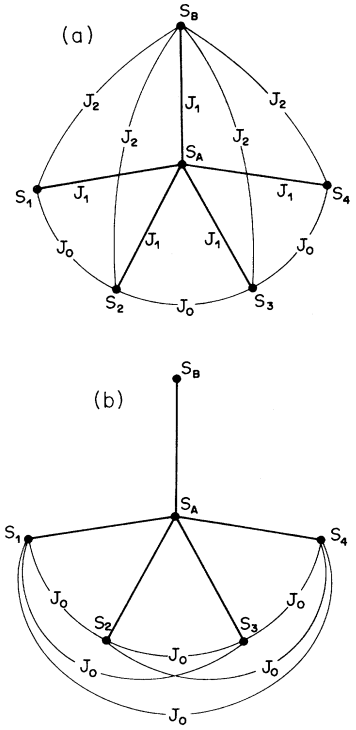

FIG. 2. (a) Spin interactions in the SR model on a tree of coordination $z=5$. The ferromagnetic J_0 interactions are along a chain of spins belonging to the same generation and with the common ancestor S_A. (b) Ferromagnetic J_0 interactions in the LR model.

be written as

$$f(S_A,S_B)=C\exp\{US_A+VS_B+WS_AS_B\}\ , \tag{2.4}$$

where

$$C^4=f(1,1)f(1,-1)f(-1,1)f(-1,-1)\ , \tag{2.5a}$$

$$U=U(K_1,K_2,H,K_0)=\frac{1}{4}\ln\left[\frac{f(1,1)f(1,-1)}{f(-1,1)f(-1,-1)}\right]\ , \tag{2.5b}$$

$$V=V(K_1,K_2,H,K_0)=\frac{1}{4}\ln\left[\frac{f(1,1)f(-1,1)}{f(1,-1)f(-1,-1)}\right]\ , \tag{2.5c}$$

$$W=W(K_1,K_2,H,K_0)=\frac{1}{4}\ln\left[\frac{f(1,1)f(-1,-1)}{f(-1,1)f(1,-1)}\right]\ . \tag{2.5d}$$

There are two effective fields associated with spins S_A and S_B and an effective interaction between spins on sites A and B. The application of this decimation scheme to successive generations of the tree yields the recursion relations

$$X_n=H+U(Y_{n-1},K_2,X_{n-1},K_0)+(z-1)V(Y_{n-2},K_2,X_{n-2},K_0) \tag{2.6a}$$

and

$$Y_n=K_1+W(Y_{n-1},K_2,X_{n-1},K_0)\ , \tag{2.6b}$$

where X_n is the effective field associated with the nth generation and Y_n is the effective interaction between spins belonging to generations n and $n+1$.

Equations (2.6a) and (2.6b) are a three-dimensional nonlinear map. In the limit of infinite coordination $z\to\infty$, $J_1\to 0$, $J_2\to 0$, with zJ_1 and z^2J_2 fixed, this map is considerably simplified. To take this limit, let us expand $\ln f(S_A,S_B)$ in powers of K_1 and K_2,

$$\ln f(S_A,S_B)=\ln f_0+(K_1S_A+K_2S_B)(z-1)m+O(K_1^2,K_2^2)\ , \tag{2.7}$$

where f_0 is the function $f(S_A,S_B)$ for $K_1=K_2=0$ and $(z-1)m=\partial f_0/\partial H$, where $m=m(H)$ is an effective magnetization per spin on a generation of the tree. Inserting this expansion into Eqs. (2.5), in the infinite-coordination limit, we obtain $U=zK_1m$, $V=zK_2m$, and $W=0$. As W vanishes, the problem is reduced to the two-dimensional map

$$X_n=H+zK_1m(X_{n-1})+z^2K_2m(X_{n-2})\ . \tag{2.8}$$

Introducing the dimensionless parameters

$$t=\frac{k_BT}{zJ_1}\ , \tag{2.9a}$$

$$p=-\frac{z^2J_2}{zJ_1}\ , \tag{2.9b}$$

and

$$b=\frac{h}{zJ_1}\ , \tag{2.9c}$$

we can rewrite Eq. (2.8) in the simpler form

$$X_n=\frac{1}{t}\{m(X_{n-1})-pm(X_{n-2})+b\}\ . \tag{2.10}$$

The effective magnetization per spin associated with the nth generation, $m_n=g(X_n)$, is an odd function of the effective field X_n. Also, as it is bounded between -1 and $+1$, it is convenient to write the map in the form

$$m_n=g\left[\frac{1}{t}m_{m-1}-\frac{p}{t}m_{m-2}+\frac{b}{t}\right]\ . \tag{2.11}$$

From the analysis of the attractors of these recursion relations, we obtain the phase diagrams of the models. The particular form of the function $g(X)$ depends on the special model under consideration. In this paper we restrict our analysis to $b=0$, which corresponds to a physical situation in the absence of an applied magnetic field.

III. ANALYTICAL RESULTS FOR THE RECURSION RELATIONS

In zero field, depending on the parameters of the model, the recursion relations are associated with the following attractors: (i) a trivial paramagnetic fixed point

$m^*=0$; (ii) a ferromagnetic fixed point $m^*\neq 0$; (iii) a periodic cycle $m_{n+L}=m_L$, for all n, corresponding to a commensurate modulated phase with period L; (iv) a one-dimensional orbit, corresponding to an incommensurate phase. Because of the limitations of the numerical calculations, however, it is difficult to distinguish an incommensurate from the commensurate phases with very large values of the period L; (v) a strange attractor, with sensitive dependence on the initial conditions, associated with the possible existence of a chaotic phase.

In the linear approximation, the recursion relations can be written as

$$\begin{bmatrix} dm_n \\ dm_{n-1} \end{bmatrix} = R_n \begin{bmatrix} dm_{n-1} \\ dm_{n-2} \end{bmatrix} , \tag{3.1}$$

where the matrix R_n is given by

$$R_n = \begin{bmatrix} \frac{1}{t}g'(X_n) & -\frac{p}{t}g'(X_n) \\ 1 & 0 \end{bmatrix} . \tag{3.2}$$

To analyze the linear stability of the solutions, we consider the eigenvalues of the matrix

$$R^N = \prod_{n=1}^{N} R_n , \tag{3.3}$$

where $N=1$ for the paramagnetic and ferromagnetic fixed points and $N=L$ for the cycles of period L. To investigate the stability of one-dimensional orbits and strange attractors, we take the limit $N\to\infty$. The Lyapunov numbers are defined as

$$\alpha_i = |\lambda^i(N)|^{1/N} , \tag{3.4}$$

where λ^i is the ith eigenvalue of the matrix R^N. The periodic cycles are associated with $\alpha_i<1$ for all i. For the one-dimensional orbits, one of the Lyapunov numbers is unity, but the other is smaller. The strange attractors are characterized by a Lyapunov number larger than unity.

On the basis of the analysis of the linear stability of the trivial paramagnetic fixed point $m^*=0$, we come to the following conclusions.

(i) For $p<g'(0)/4t$ and $1-p<t/g'(0)$, the paramagnetic fixed point is stable, with real eigenvalues.

(ii) For $p>g'(0)/4t$ and $p<t/g'(0)$, the paramagnetic fixed point is stable with complex eigenvalues.

The first conditions are associated with a paramagnetic-ferromagnetic phase transition. The second conditions indicate a transition to a modulated phase. There is also a Lifshitz point, given by $p=\frac{1}{2}$ and $t=g'(0)/2$.

The ferromagnetic fixed point $m^*\neq 0$ comes from the solution of the equation

$$m^*=g(X^*) , \tag{3.5a}$$

with

$$X^*=\frac{1}{t}(1-p)m^* . \tag{3.5b}$$

The analysis of the linear stability of the ferromagnetic fixed point leads to the following conclusions.

(iii) For $p<g'(X^*)/4t$ and $(1-p)<t/g'(X^*)$, the ferromagnetic fixed point is stable with real eigenvalues.

(iv) For $p>g'(X^*)/4t$ and $p<t/g'(X^*)$, the ferromagnetic fixed point is stable with complex eigenvalues. The values of m^* are determined numerically. However, near the paramagnetic border, m^* is small, and as $g(X)$ is an odd function, we have the expansions

$$m^*=g'(0)X^*+\tfrac{1}{6}g'''(0)(X^*)^3+\cdots \tag{3.6a}$$

and

$$g'(X^*)=g'(0)=\tfrac{1}{2}g'''(0)(X^*)^2+\cdots . \tag{3.6b}$$

Condition (iii) for the stability of the ferromagnetic fixed point is then reduced to $p<g'(0)/4t$ and $tg'(0)<1-p$. Comparing with the conditions for the stability of the paramagnetic fixed point, we show the continuous nature of the paramagnetic-ferromagnetic phase transition.

In the modulated phase, very close to the paramagnetic region, we can write the recursion relations in the linear form

$$m_n=\frac{1}{t}g'(0)[m_{n-1}-pm_{n-2}] . \tag{3.7}$$

Using the representation

$$m_n=\sum_q m_q \exp(iqn) , \tag{3.8}$$

in terms of the wave number q, we see that the paramagnetic-modulated transition, given by the condition $p=t/g'(0)$, is also of second order. The critical wave number, given by the relation $\cos q_c=1/2p$, vanishes at the Lifshitz point.

In the basic model studied by Yokoi, de Oliveira, and Salinas,[15] with $J_0=0$, we have $g(X)=\tanh(X)$. Our analytical results agree with the calculations for this model. Let us then consider the specific cases of the LR and SR models.

A. SR model

In the Sr model, the short-range $J_0>0$ interactions give rise to an Ising chain of spins [see Fig. 2(a)]. In the infinite-coordination limit, the function $g(X)$ is given by the usual expression for the magnetization per spin of an Ising chain:

$$g(X)=\tanh(X)\{\exp(-4K_0) + [1-\exp(-4K_0)]\tanh^2 X\}^{-1/2} . \tag{3.9}$$

The two-dimensional map associated with the SR model is given by

$$m_n=\tanh\left[\frac{1}{t}m_{n-1}-\frac{p}{t}m_{n-2}\right]\left\{\exp\left[-\frac{4r}{t}\right]+\left[1-\exp\left[-\frac{4r}{t}\right]\right]\tanh^2\left[\frac{1}{t}m_{n-1}-\frac{p}{t}m_{n-2}\right]\right\}^{-1/2} , \tag{3.10}$$

where $r=J_0/zJ_1$. For $p<\frac{1}{2}$ the paramagnetic-ferromagnetic transition is given by $t\exp(-2r/t)=1-p$. For $p>\frac{1}{2}$ the paramagnetic-modulated transition is given by $t\exp(-2r/t)=p$. The Lifshitz point is located at $p=\frac{1}{2}$ with $2t\exp(-2r/t)=1$.

B. LR model

In the LR model, there are long-range $J_0>0$ interactions between all pairs of spins belonging to the group of sites on the same generation with the same ancestor site along the tree [see Fig. 2(b)]. In the infinite-coordination limit, we take $J_0\to 0$, $z\to\infty$, with zJ_0 fixed. The function $g(X)$ is then given by the well-known mean-field expression

$$g(X)=\tanh(zK_0m+X)\ . \tag{3.11}$$

Thus we have the map

$$m_n=\tanh\left[\frac{s}{t}m_n+\frac{1}{t}m_{n-1}-\frac{p}{t}m_{n-2}\right]\ , \tag{3.12}$$

where $s=zJ_0/zJ_1$. For $p<\frac{1}{2}$ the paramagnetic-ferromagnetic transition is given by $t=1-p+s$. For $p>\frac{1}{2}$ the paramagnetic-modulated transition is given by $t=p+s$. The Lifshitz condition becomes $p=\frac{1}{2}$ with $t=\frac{1}{2}+s$.

IV. NUMERICAL CALCULATIONS FOR THE SR MODEL

Taking advantage of the simple structure of the map, given by Eq. (3.10), we have performed some detailed numerical calculations for the SR model. Given the initial conditions (which are usually, but not necessarily, taken as $m_1=m_2=1$) and the parameters t, p, and r, we can plot graphs of $m_{n-1}\times m_{n-2}$, for $n=3,4,5,\ldots$. After discarding some initial data, the flows in these plots converge to a certain type of attractor. For the commensurate modulated phases, we define a principal wave number, given by $q=(l+1)/2L$ in units of 2π, where l is the number of times the effective magnetization per spin changes sign during the period L.

In Fig. 3 we show the t-p phase diagram of the SR model with $r=0.1$. Similar diagrams can be obtained for other positive values of the parameter r. Only the main commensurate phases are indicated in this picture. It should be understood that in between these phases there are many other commensurate phases with larger periods. As in the basic model,[15] the paramagnetic lines do not meet smoothly at the Lifshitz point. At the multiphase point $t=0$ and $p=1$, the transition lines have an infinite slope, as in the ANNNI model on a cubic lattice.[3] The small dark region indicates the presence of stable ferromagnetic and modulated attractors, which can be reached depending on the particular set of initial conditions. As there is no expression for the free energy of these models, we have not been able to determine the first-order boundary between the ferromagnetic and modulated phases. Inside the region of coexisting solutions, we present some numerical evidence to support the existence of a strange attractor, with a positive Lyapunov exponent $\gamma=\ln\alpha>0$. In Table I, for $r=0.1$ and $t=0.25$, we list the modulated phases in a small range of p within the region of coexisting solutions.

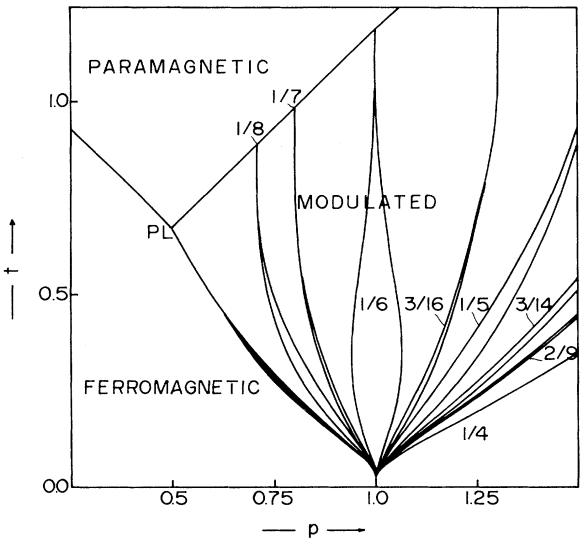

FIG. 3. General features of the t-p phase diagram of the SR model with $r=0.1$. PL is a Lifshitz point. In the modulated region, we show a few commensurate phases, indicated by the corresponding principal wave numbers. In the dark region, there is a coexistence between ferromagnetic and modulated attractors of the map.

In Fig. 4, for $r=0.1$, $t=0.25$, and $p=0.776$, we show a strange attractor, with Lyapunov exponents $\gamma_1=0.1131$ and $\gamma_2=-1.0598$, obtained by using an algorithm proposed by Eckmann and Ruelle.[16] From the Kaplan-Yorke conjecture,[17] we estimate the Lyapunov dimension $D_L=1.107$, which indicates the fractal character of this strange attractor. It should be pointed out, however, that recent calculations for the basic model show that the Lyapunov dimension is slightly different from the box-counting Hausdorff dimension.[18] The strange attractor comes from a sequence of bifurcations of a modulated phase. For example, in Table I we see that the $\frac{8}{104}$ phase comes from a three-duplication of the $\frac{1}{13}$ phase. For intermediate values of p, we find the $\frac{2}{26}$ and $\frac{4}{52}$ phases. This same pattern occurs for the $\frac{1}{14}$ phase, as we note the existence of the $\frac{3}{42}$ phase localized in a window inside the chaotic region. For the similar strange attractor in the basic model, Yokoi, de Oliveira, and Salinas[15] have calculated a route to chaos according to the scenario of Feigenbaum.

In the modulated region, for large enough p, we find the $\frac{1}{4}$ commensurate phase, corresponding to a sequence of the type $++--$, of two positive followed by two negative values of the effective magnetization per spin along the generations of the tree. For $p=1$, from the multiphase point up to the paramagnetic border, we find the $\frac{1}{6}$ modulated structure ($+++---$). Between the $\frac{1}{6}$ and $\frac{1}{4}$ phases, we obtain many combinations of these structures. Our numerical calculations, however, do not

indicate the existence of a well-defined branching process.[10]

In Fig. 5, for $r=0.1$ and $t=0.1$, we show the Lyapunov number as a function of p in the interior of the $\frac{1}{6}$ phase. At the borders of this phase, the Lyapunov number goes to unity. This shows that, even at low temperatures, there is room for the existence of incommensurate phases. For $p>1$ the $\frac{1}{6}$ phase is present up to $p=1.018\,99$. At $p=1.019\,00$ we find the $\frac{361}{2160}$ phase (which means that a structure of the type $++$ appears 6 times during a period of 2160 generations). For $p<1$, near the $\frac{1}{6}$ phase, there is a $\frac{86}{517}$ phase, where a structure of the type $++++$ appears only once during a period of 517 generations. A more detailed analysis of the interval between these phases supports the existence of additional commensurate phases characterized by intermediate rational numbers.

TABLE I. Sequence of phases for the SR model with $r=0.1$, $t=0.25$, and the initial conditions $m_1=m_2=1$. The range of values of p corresponds to a narrow region of coexisting ferromagnetic and modulated attractors. The modulated structures are indicated by the principal wave number. The third column gives the largest Lyapunov exponent.

p	Phase	γ_1
0.7734	ferromagnetic	−0.0999
0.7735	chaotic	0.1747
0.7736	$\frac{3}{44}$	−0.0164
0.7737	$\frac{1}{15}$	−0.2223
0.7738	chaotic	0.1336
0.7739	chaotic	0.1501
0.7740	$\frac{1}{16}$	−0.8831
0.7741	chaotic	0.1001
0.7742	chaotic	0.1106
0.7743	chaotic	0.1087
0.7744	chaotic	0.0305
0.7745	chaotic	0.1150
0.7746	chaotic	0.0999
0.7747	$\frac{1}{13}$	−0.1459
0.7748	$\frac{8}{104}$	−0.1554
0.7749	chaotic	0.0913
0.7750	chaotic	0.0467
0.7751	chaotic	0.1027
0.7752	chaotic	0.1045
0.7753	chaotic	0.1185
0.7754	chaotic	0.1084
0.7755	$\frac{3}{42}$	−0.0033
0.7756	$\frac{4}{56}$	−0.0063
0.7757	$\frac{1}{14}$	−0.2172
0.7758	$\frac{1}{14}$	−0.0352
0.7759	$\frac{1}{14}$	−0.4118
0.7760	chaotic	0.1153
0.7761	chaotic	0.0965
0.7762	chaotic	0.0985
0.7763	chaotic	0.0881
0.7764	chaotic	0.0776
0.7765	chaotic	0.0764
0.7766	chaotic	0.0755
0.7767	chaotic	0.0580
0.7768	$\frac{1}{12}$	−0.0999

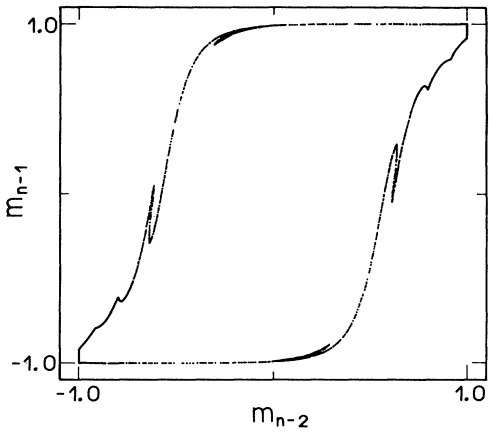

FIG. 4. Plot of a strange attractor of the SR model for $t=0.25$, $p=0.776$, and $r=0.1$. The associated Lyapunov dimension is $D_L=1.107$.

At high temperatures the incommensurate phases are associated with densily closed orbits in the $m_{n-1}\times m_{n-2}$ plots. At lower temperatures, however, there are incommensurate phases associated with "dashed" attractors, as shown in Fig. 6, for $r=0.1$, $t=0.2$, and $p=1.050\,073$, near to the $\frac{1}{6}$ phase. In this picture we have plotted 40 000 points. The inset shows a densily populated dash of the attractor. Both types of incommensurate phases are characterized by at least one Lyapunov number $\alpha_1=1$. The closed orbits are associated with unpinned incommensurate phases. The dashed attractors correspond to a pinned incommensurate phase.[19]

At fixed t the principal wave number of the modulated phases as a function of p displays a devil's staircase shape,[4] as shown in Fig. 7 for $r=0.1$. At low temperatures the commensurate steps occupy the full range of

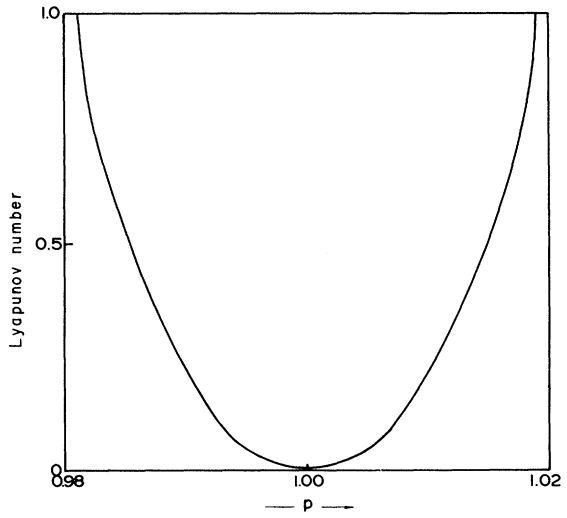

FIG. 5. Graph of the largest Lyapunov number of the SR model as a function of the parameter p inside the $\frac{1}{6}$ phase (for $t=0.1$ and $r=0.1$).

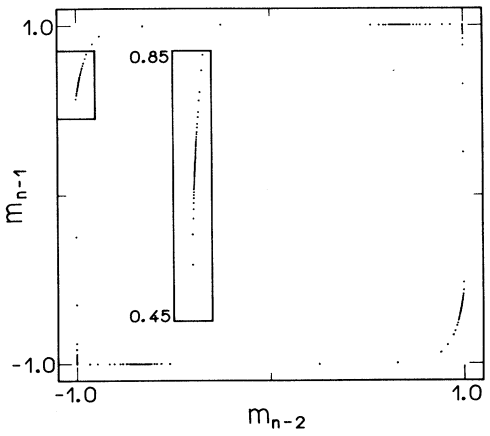

FIG. 6. Plot of the attractor associated with a pinned incommensurate phase of the SR model (for $t=0.2$, $r=0.1$, and $p=1.050\,073$). In this graph we plot 40 000 iterations after discarding a small transient. The inset shows a densily populated dash of the attractor.

values of p. At high temperatures, however, the width of the steps is reduced, and the incommensurate phases occupy a range of finite measure. It is easy to calculate the fractal Hausdorff dimension D_F of the set of points between the steps.[20,21] Using the scale ε, suppose the steps occupy a total length $S(\varepsilon)$ between two given values of p. The set of points between the steps has the length $L(\varepsilon)=C-S(\varepsilon)$, where C is the total length of the interval under consideration. The fractal dimension is given by the slope of the graphs $\ln[L(\varepsilon)/\varepsilon]\times \ln(1/\varepsilon)$, for small values of the length scale ε. Table II presents some results for several temperatures. For $D_F<1$ the incommensurate phases have zero measure and the devil's staircases are complete. For increasing temperatures, $D_F\to 1$. Thus there is numerical evidence to show that, at high temperatures, the incommensurate phases occupy finite portions of the phase diagram and the devil's staircases become incomplete.

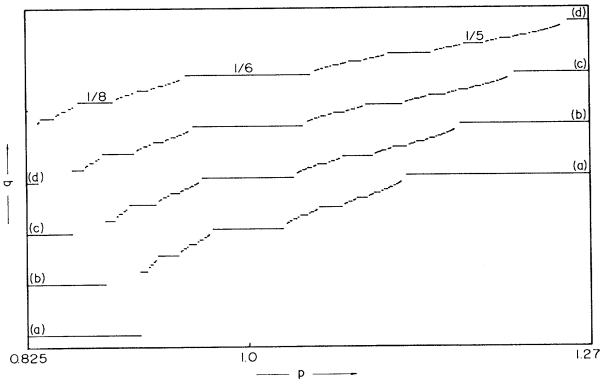

FIG. 7. Graphs of the principal wave number as a function of the competition parameter p for SR model with $r=0.1$ and different values of the temperature: (a) $t=0.125$, (b) $t=0.15$, (c) $t=0.175$, and (d) $t=0.2$. We show all steps with $\Delta p>3\times 10^{-4}$. The Hausdorff dimensionalities of the devil's staircases are given in Table II.

TABLE II. Hausdorff dimensionalities as a function of temperature. D_F(SR) is associated with the SR model for $r=0.1$. D_F(LR) is associated with the LR model for $s=0.2$ (See Figs. 7 and 12). The parentheses indicate the errors from the best fitting to a straight line.

t	D_F(SR)	D_F(LR)
0.1	0.82(1)	0.40(2)
0.125	0.84(1)	0.46(3)
0.15	0.88(1)	0.71(3)
0.175	0.91(1)	0.957(6)
0.2	0.93(1)	0.970(5)
0.225	0.954(7)	
0.25	0.969(6)	

V. NUMERICAL CALCULATIONS FOR THE LR MODEL

The numerical analysis of the LR model, based on the map given by Eq. (3.12), is more difficult, as m_n shows up in the argument of the hyperbolic tangent. At each step of the iteration, given m_{n-1} and m_{n-2}, the value of m_n comes from the solution of a transcendental equation. The computational time is thus considerably increased, and we have not tried to perform an analysis as detailed as in the case of SR model. However, in general we obtain very similar results. The ferromagnetic-modulated transition is still of first order, with the coexistence of modulated (or chaotic) and ferromagnetic solutions in a narrow region of the phase diagram. At high temperatures, the incommensurate structures predominate. At low temperatures, in addition to the commensurate phases, there is also numerical evidence to support the existence of pinned incommensurate phases.

As there are long-range interactions between pairs of spins belonging to the same generation, in the infinite-coordination limit the LR model displays a novel mean-field ordering within each generation. This long-range effect is responsible for the main differences between the LR and both the SR and basic models. From this point of view, the LR model is much closer to the mean-field ANNNI model on a Bravais lattice.[22,23] To illustrate the differences among these models, consider the $\frac{1}{6}$ phase for $p=1$. At low temperatures, for $m_{n-1}=m_{n-2}$, from Eq. (2.10) we obtain $X_n=0$. In this case, for both the basic and SR models, we have $m_n=0$, and the $\frac{1}{6}$ phase is given by the sequence $++0--0$. For the LR model, however, we may have $m_n\neq 0$ even with $X_n=0$. In Fig. 8 we consider the $\frac{1}{6}$ phase of the LR model, with $p=1$ and for three different values of the parameter s. The graphs display the effective magnetization per spin along three successive generations of the tree as a function of temperature. For $s=0.2$ and $t<0.14$, all three magnetizations are different from zero. In this case we have a structure of the type $+++---$, with equal magnetizations in the first and third generations. For $t>0.2$ we obtain the same structure as in the SR and basic models, with the existence of many generations with a vanishing magnetization. For $0.14<t<0.2$, we obtain another structure where all magnetizations are different, the first magnetization going to zero at $t=0.2$. Similar features occur for

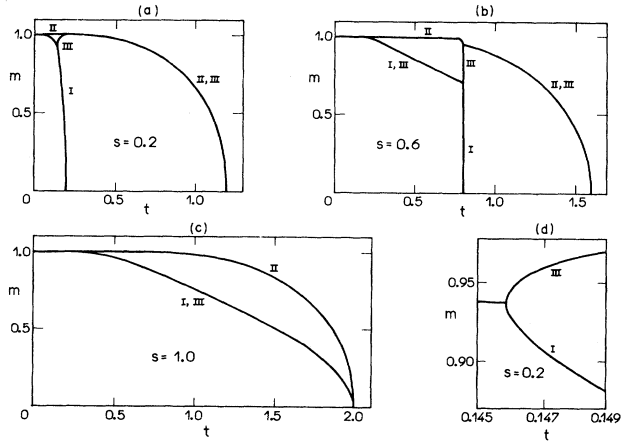

FIG. 8. Plots of the effective magnetization per spin the $\frac{1}{6}$ phase of the LR model along three successive generations of the tree, I, II, and III, for $p=1$, and different values of the parameter $s=J_0/J_1$. In (a) and (b), for $s=0.2$ and $s=0.6$, respectively, the effective magnetization m_{I} vanishes above a certain temperature (while m_{II} and m_{III} are still positive). For $s=1.0$ all three successive magnetizations vanish at the same (paramagnetic) critical temperature. (d) A detail of the bifurcation in (a).

$s=0.6$, the structures with zero magnetization showing up for $t>0.8$. For $s=0.1$, however, there is no longer a structure with zero magnetization. The ANNNI model also shows this kind of behavior. The A, B, and C phases found by Yokoi[23] are directly related to our phases for $t<0.14$, $t>0.20$, and $0.14<t<0.20$, with $s=0.2$, respectively.

As we have remarked in the last paragraph, the parameter s changes important features of the behavior of the LR model. In Figs. 9 and 10, we show t-p phase diagrams for $s=0.2$ and 1.0. The main qualitative difference between these phase diagrams is illustrated in Fig. 11 for $s=0.2$. The $\frac{1}{6}$ region displays a bottleneck with a pronounced narrowing at $t\approx 0.16$. The dashed line indicate the transitions between the characteristic A, C, and B structures of the $\frac{1}{6}$ phase [compare with Figs.

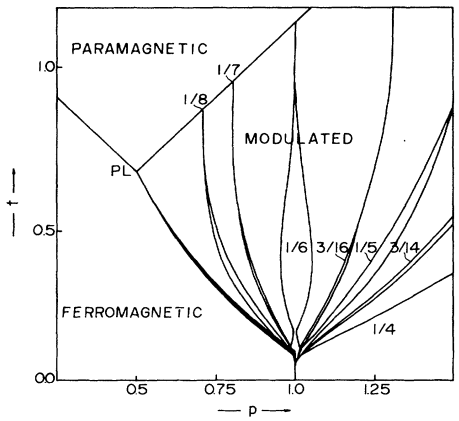

FIG. 9. General features of the t-p phase diagram of the LR model for $s=0.2$. The region of the $\frac{1}{6}$ phase shows a typical bottleneck at $t\approx 0.2$.

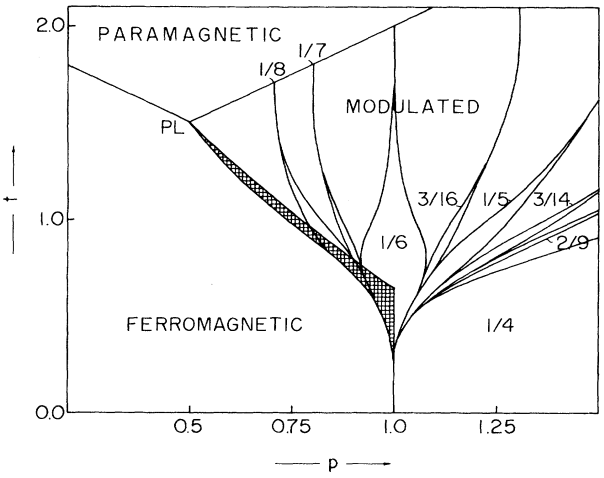

FIG. 10. General features of the t-p phase diagram of the LR model for $s=1.0$. The shaded region indicates the coexistence of ferromagnetic and modulated attractors.

8(a) and 8(d) for $p=1$]. At higher temperatures the B structure $++0--0$ predominates and the $\frac{1}{6}$ region broadens again.

In Fig. 12 we show some devil's staircases for $s=0.2$. At the characteristic temperature $t=0.15$, we see a large number of small steps associated with the presence of long-period modulated phases. At high temperatures many small steps disappear, and the short-period modulated phases begin to predominate. The values of the fractal dimensionalities in Table II illustrate these features of the LR model.

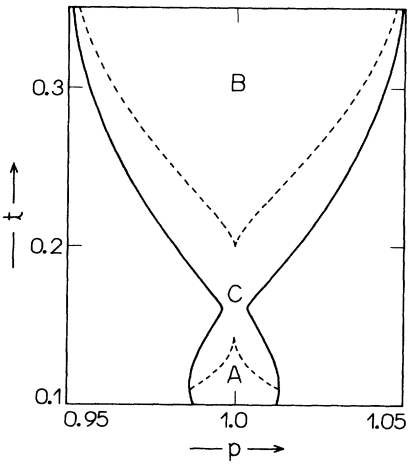

FIG. 11. Detail of the t-p phase diagram of the LR model for $s=0.2$ (see Fig. 9). There is a pronounced narrowing of the $\frac{1}{6}$ region for $t\approx 0.16$. The dashed lines indicate the transitions between the characteristic structures of the $\frac{1}{6}$ phase [see Figs. 8(a) and 8(d), for $p=1$]. At higher temperatures the B structure predominates and the $\frac{1}{6}$ region broadens again.

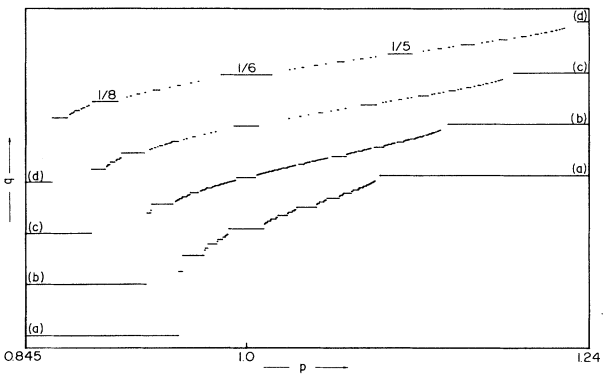

FIG. 12. Graphs of the principal wave number as a function of p for the LR model with $s=0.2$ and (a) $t=0.125$, (b) $t=0.15$, (c) $t=0.175$, and (d) $t=0.2$. We draw all steps with $\Delta p > 3\times 10^{-4}$.

VI. CONCLUSIONS

We have introduced two analogs of the ANNNI model on a Cayley tree. Besides the competing interactions between first and second neighbors along the branches of the tree, we have included some ferromagnetic interactions between pairs of spins belonging to the same generations. These extra ferromagnetic interactions were introduced to mimic the x-y planes of the ANNNI model on a cubic lattice.

Depending on the nature of the in-generation ferromagnetic interactions, we define short- and long-range models. Although identical for a tree of coordination $z=3$, some features of these models become quite distinct as the coordination increases. The statistical problem on a Cayley tree can be formulated as a discrete nonlinear map. Given the boundary conditions and the model parameters, the phases of the system are defined by the attractors of the map, which correspond to solutions on the Bethe lattice, deep inside a large Cayley tree. In the infinite-coordination limit, the maps become two dimensional and the problem is considerably simplified. We have taken advantage of this simplification to perform some analytical as well as detailed numerical calculations.

We have obtained expressions for the paramagnetic lines and the location of a Lifshitz and a multiphase point in the t-p phase diagrams. Besides the paramagnetic and ferromagnetic regions, there are large portions of the phase diagrams occupied by sequences of modulated structures, characterized by a principal wave number q. At low temperatures the graphs of q against the competition parameter p display the typical shape of a devil's staircase. We have performed numerical calculations to show that these staircases are complete, with Hausdorff dimensionalities increasing with temperature. At high temperatures the incommensurate phases are expected to occupy finite portions of the modulated region of the phases diagrams.

We have investigated several additional details of the phase diagram of the SR model. For example, near to the ferromagnetic border, we have performed numerical calculations of the Lyapunov exponents to support the existence of a region of chaotic phases, associated with a strange attractor of the map, with Lyapunov dimension $D_L > 1$. The main features of the incommensurate phases have also been investigated. At high temperatures they are associated with densily populated closed orbits, with a vanishing Lyapunov exponent. At low temperatures, although still associated with a vanishing Lyapunov exponent, there are pinned incommensurate structures, characterized by dashed attractors.

In the LR model, for small in-generation ferromagnetic interactions, the main modulated phases undergo a transition from characteristic structures at low and high temperatures. This same kind of phenomenon, which is associated with weak in-plane ferromagnetic interactions, has also been found in the mean-field calculations for the ANNNI model on a cubic lattice.

[1]W. Selke and M. E. Fisher, Phys. Rev. B **20**, 257 (1979).
[2]P. Bak and J. von Boehm, Phys. Rev. B **21**, 5279 (1980).
[3]M. E. Fisher and W. Selke, Phys. Rev. Lett. **44**, 1502 (1980); Philos. Trans. R. Soc. London **302**, 1 (1981).
[4]P. Bak, Rep. Prog. Phys. **45**, 587 (1982).
[5]W. Selke, Phys. Rep. **170**, 213 (1988).
[6]J. M. Yeomans, in *Solid State Physics,* edited by H. Ehrenreich and D. Turnbull (Academic, Orlando, 1988), Vol. 41.
[7]W. Selke, in *Phase Transitions and Critical Phenomena,* edited by C. Domb and J. L. Lebowitz (Academic, London, 1992), Vol. 15.
[8]S. Redner and H. E. Stanley, Phys. Rev. B **16**, 4901 (1977).
[9]C. S. O. Yokoi, M. D. Coutinho-Filho, and S. R. Salinas, Phys. Rev. B **24**, 4047 (1981).
[10]W. Selke and P. M. Duxbury, Z. Phys. B **57**, 49 (1984); J. Phys. A **16**, L741 (1983).
[11]M. J. Jensen and P. Bak, Phys. Rev. B **29**, 6280 (1983).
[12]J. Vannimenus, Z. Phys. B **43**, 141 (1981).
[13]S. Inawashiro, C. J. Thompson, and G. Honda, J. Stat. Phys. **33**, 419 (1983).
[14]A. M. Mariz, C. Tsallis, and E. L. Albuquerque, J. Stat. Phys. **40**, 577 (1985).
[15]C. S. O. Yokoi, M. J. de Oliveira, and S. R. Salinas, Phys. Rev. Lett. **54**, 163 (1985).
[16]J.-P. Eckmann and D. Ruelle, Rev. Mod. Phys. **57**, 617 (1985).
[17]J. D. Framer, E. Ott, and A. L. Yorke, Physica D **7**, 153 (1983).
[18]C. P. C. Prado and N. Fiedler-Ferrari, Phys. Lett. A **135**, 175 (1989).
[19]W. Li and P. Bak, Phys. Rev. Lett. **57**, 655 (1986).
[20]M. J. Jensen, P. Bak, and T. Bohr, Phys. Rev. Lett. **50**, 1637 (1983).
[21]C. S. O. Yokoi and M. J. de Oliveira, J. Phys. A **18**, L153 (1985); T. Tome and S. R. Salinas, *ibid.* **20**, L311 (1988).
[22]K. Nakanishi, J. Phys. Soc. Jpn. **58**, 1296 (1989).
[23]C. S. O. Yokoi, Phys. Rev. B **43**, 8487 (1991).